Journal of Applied Mathematics and Physics, 2024, 12, 488-508
https://www.scirp.org/journal/jamp
ISSN Online: 2327-4379
ISSN Print: 2327-4352

Heteroclinic Cycles in a Class of 3-Dimensional Piecewise Affine Systems

Minghao Liu, Ruimin Liu

School of Mathematical Sciences, School of Mathematical Sciences, Shandong Normal University, Jinan, China
Email: 18463426969@163.com, 17860509460@163.com

How to cite this paper: Liu, M.H. and Liu, R.M. (2024) Heteroclinic Cycles in a Class of 3-Dimensional Piecewise Affine Systems. *Journal of Applied Mathematics and Physics*, **12**, 488-508.
https://doi.org/10.4236/jamp.2024.122033

Received: January 12, 2024
Accepted: February 26, 2024
Published: February 29, 2024

Abstract

This paper explores the existence of heteroclinic cycles and corresponding chaotic dynamics in a class of 3-dimensional two-zone piecewise affine systems. Moreover, the heteroclinic cycles connect two saddle foci and intersect the switching manifold at two points and the switching manifold is composed of two perpendicular planes.

Keywords

Piecewise Affine System, Heteroclinic Cycle, Chaotic Invariant Set

1. Introduction

Since the introduction of the Lorenz system as a highly simplified model for atmospheric convection in [1], extensive research has been conducted on chaos phenomena. The development of chaos generators has significant potential for various engineering applications. Hybrid systems have recently garnered considerable attention due to their critical role in circuit design, control theory, computer science, and biological molecular networks [2] [3] [4] [5] [6]. However, establishing the existence of singular cycles in general dynamical systems is challenging, as analytical calculations of invariant manifolds and solutions are not feasible [7] [8] [9] [10].

Thankfully, it is possible to analytically determine the invariant manifolds and solutions of linear systems. This allows for the mathematical construction of piecewise affine systems with singular cycles, which can be utilized in chaotic generator design [11] [12]. Nevertheless, investigating the presence of singular cycles in general piecewise linear systems is not straightforward, as it involves detecting return times and potential intersections of singular cycles with switching planes, which is a complex task [6] [13] [14]. For instance, in [15], the pri-

mary focus was on creating double-scroll chaotic generators by exploring the existence of heteroclinic cycles connecting two saddle-focus points and the associated chaotic dynamics in a specific class of 3-dimensional piecewise affine systems with a switching plane. Additionally, in [6], the authors examined the existence of homoclinic orbits to saddle-focus and the resulting chaotic dynamics in 3-dimensional continuous piecewise linear systems in normal forms, with three parameters and a switching plane. Similarly, references [16] [17] investigated the existence of homoclinic orbits to saddle-focus and the corresponding chaotic dynamics in a specific class of 3-dimensional piecewise affine systems with a switching plane. Reference [18] delved into the existence of heteroclinic cycles that intersect two or three regions in a particular class of 3-dimensional three-zone piecewise affine systems with two switching planes. In reference [19], the authors investigated multiple categories of planar piecewise Hamiltonian systems that feature three zones separated by two parallel straight lines. Reference [20] focuses on the study of external bifurcations of heterodimensional cycles in a 3-dimensional vector field. These cycles connect three saddle points and exhibit an orbit flip, forming a shape resembling the symbol "∞". In references [21] [22] [23], the authors offered sufficient conditions for the coexistence of two singular cycles and the related chaotic dynamics in 3-dimensional two-zone piecewise linear systems with two parallel switching planes. Furthermore, they discovered that the coexistence of singular cycles could lead to a wider range of chaotic dynamics.

This paper is organized as follows. Section 2 gives some preliminaries of the 3-dimensional piecewise affine systems. Section 3 states the main results of this paper. Section 4 presents the proof of Theorem 1. Section 5 presents the proof of Theorem 2.

2. Statement of the Problem

Consider the 3-dimensional piecewise affine systems

$$\dot{\boldsymbol{x}} = \begin{cases} \boldsymbol{A}\boldsymbol{x} + \boldsymbol{a}, & \boldsymbol{x} \in \Sigma_+, \\ \boldsymbol{B}\boldsymbol{x} + \boldsymbol{b}, & \boldsymbol{x} \in \Sigma_-, \end{cases} \tag{1}$$

where $\boldsymbol{x} = (x, y, z) \in \mathbb{R}^3$, $\boldsymbol{a}, \boldsymbol{b}$ are constant vectors in $\mathbb{R}^3$, $\boldsymbol{A}, \boldsymbol{B}$ are constant matrices in $\mathbb{R}^{3\times 3}$. The eigenvalues of $\boldsymbol{A}$ are $\alpha_1 \pm \beta_1$, λ_1 with β_1, $\lambda_1 > 0$, $\alpha_1 < 0$, and the eigenvalues of $\boldsymbol{B}$ are $\alpha_2 \pm \beta_2$, λ_2 with β_2, $\lambda_2 > 0$, $\alpha_2 < 0$. Moreover, there exist invertible matrices P and Q such that

$$\boldsymbol{A} = PJ_1P^{-1}, \boldsymbol{B} = QJ_2Q^{-1}, \tag{2}$$

where matrices P and Q are given by

$$P = (\zeta_1 \quad \zeta_2 \quad \zeta_3), \ Q = (\xi_1 \quad \xi_2 \quad \xi_3),$$

with ζ_i and ξ_i $(i = 1,2,3)$ being the generalized eigenvector of matrices $\boldsymbol{A}$ and $\boldsymbol{B}$. In addition, we have

$$J_1=\begin{pmatrix}\alpha_1 & -\beta_1 & 0\\ \beta_1 & \alpha_1 & 0\\ 0 & 0 & \lambda_1\end{pmatrix},\ J_2=\begin{pmatrix}\alpha_2 & -\beta_2 & 0\\ \beta_2 & \alpha_2 & 0\\ 0 & 0 & \lambda_2\end{pmatrix}. \tag{3}$$

Let

$$\Sigma_+=\{(x,y,z)\,|\,y>0,z>0\},$$

$$\Sigma_-=\{(x,y,z)\,|\,y<0\}\cup\{(x,y,z)\,|\,y>0,z<0\}.$$

Denote the switching manifold of the system (1) by Σ with $\Sigma=\Sigma_1\cup\Sigma_2$, where

$$\Sigma_1=\{(x,y,z)\,|\,y=0,z\geq 0\},\ \Sigma_2=\{(x,y,z)\,|\,y>0,z=0\}.$$

Notice that $\boldsymbol{p}=-\boldsymbol{A}^{-1}\boldsymbol{a}$ is an equilibrium point of the subsystem

$$\dot{\boldsymbol{x}}=\boldsymbol{A}\boldsymbol{x}+\boldsymbol{a}, \tag{4}$$

and $\boldsymbol{q}=-\boldsymbol{B}^{-1}\boldsymbol{b}$ is an equilibrium point of the subsystem

$$\dot{\boldsymbol{x}}=\boldsymbol{B}\boldsymbol{x}+\boldsymbol{b}. \tag{5}$$

Moreover, assume that $\boldsymbol{p}\in\Sigma_+$ and $\boldsymbol{q}\in\Sigma_-$ with $\boldsymbol{p}=(x_p\ y_p\ z_p)^{\mathrm{T}}$, $\boldsymbol{q}=(x_q\ y_q\ z_q)^{\mathrm{T}}$.

From the representations of $\boldsymbol{A}$ and $\boldsymbol{B}$ in (3), the stable manifolds $W^s(\boldsymbol{p})$, $W^s(\boldsymbol{q})$ and unstable manifolds $W^u(\boldsymbol{p})$, $W^u(\boldsymbol{q})$ are expressed as

$$W^s(\boldsymbol{p})=\{\boldsymbol{p}+k_1\zeta_1+k_2\zeta_2\,|\,k_1,k_2\in\boldsymbol{R}\}, \tag{6}$$

$$W^u(\boldsymbol{p})=\{\boldsymbol{p}+k_3\zeta_3\,|\,k_3\in\boldsymbol{R}\}, \tag{7}$$

$$W^s(\boldsymbol{q})=\{\boldsymbol{q}+l_1\xi_1+l_2\xi_2\,|\,l_1,l_2\in\boldsymbol{R}\}, \tag{8}$$

$$W^u(\boldsymbol{q})=\{\boldsymbol{q}+l_3\xi_3\,|\,l_3\in\boldsymbol{R}\}. \tag{9}$$

Suppose that $\zeta_{32}\neq 0$, $\xi_{33}\neq 0$, and

$$W^u(\boldsymbol{q})\cap\Sigma_1=\left\{\boldsymbol{q}-\frac{y_q}{\xi_{32}}\xi_3\right\},\ W^u(\boldsymbol{p})\cap\Sigma_2=\left\{\boldsymbol{p}-\frac{z_p}{\zeta_{33}}\zeta_3\right\}.$$

Denote the solution of the system (4) with the initial condition $\varphi_1(0,\boldsymbol{x}_0)=\boldsymbol{x}_0$ by $\varphi_1(t,\boldsymbol{x}_0)$, and denote the solution of the system (5) with the initial condition $\varphi_2(0,\boldsymbol{y}_0)=\boldsymbol{y}_0$ by $\varphi_2(t,\boldsymbol{y}_0)$. Then we have

$$\varphi_1(t,\boldsymbol{x}_0)=\mathrm{e}^{\boldsymbol{A}t}(\boldsymbol{x}_0-\boldsymbol{p})+\boldsymbol{p},\ \varphi_2(t,\boldsymbol{y}_0)=\mathrm{e}^{\boldsymbol{B}t}(\boldsymbol{y}_0-\boldsymbol{q})+\boldsymbol{q}. \tag{10}$$

3. Main Results

In view of the method in [15] [17], this section provides some theorems on the existence of heteroclinic cycles and homoclinic orbits of systems (1). For convenience, divide the region Σ_- into three parts S_1,S_2,S_3 as shown in **Figure 1**.

In this article, we will only consider the case where the equilibrium point $\boldsymbol{q}$ is located in the S_2 region. Similar methods can be used to discuss other situations.

Let

$$\zeta_i=(\zeta_{i1}\quad\zeta_{i2}\quad\zeta_{i3})^{\mathrm{T}},\ \xi_i=(\xi_{i1}\quad\xi_{i2}\quad\xi_{i3})^{\mathrm{T}},\ i=1,2,3. \tag{11}$$

Theorem 1. If and only if System (1) exists constant real numbers k_{i0} and l_{i0}, $i=1,2$ such that the following conditions hold, then there exists a heteroclinic cycle connecting $\boldsymbol{p}$ and $\boldsymbol{q}$ that intersects Σ_1 transversally at $\boldsymbol{p}_{11}$ and intersects Σ_2 transversally at $\boldsymbol{p}_{02}$, as shown in Figure 2.

1)

$$\boldsymbol{p}_{02}=\boldsymbol{q}+l_{10}\xi_1+l_{20}\xi_2=\boldsymbol{p}-\frac{z_p}{\zeta_{33}}\zeta_3, \tag{12}$$

$$\boldsymbol{p}_{11}=\boldsymbol{q}-\frac{y_q}{\xi_{32}}\xi_3=\boldsymbol{p}+k_{10}\zeta_1+k_{20}\zeta_2, \tag{13}$$

2)

$$-\alpha_1 y_p+\beta_1\delta_2>0,\ \rho_1>-z_p,\ -\alpha_2 z_q+\beta_2\sigma_1<0, \tag{14}$$

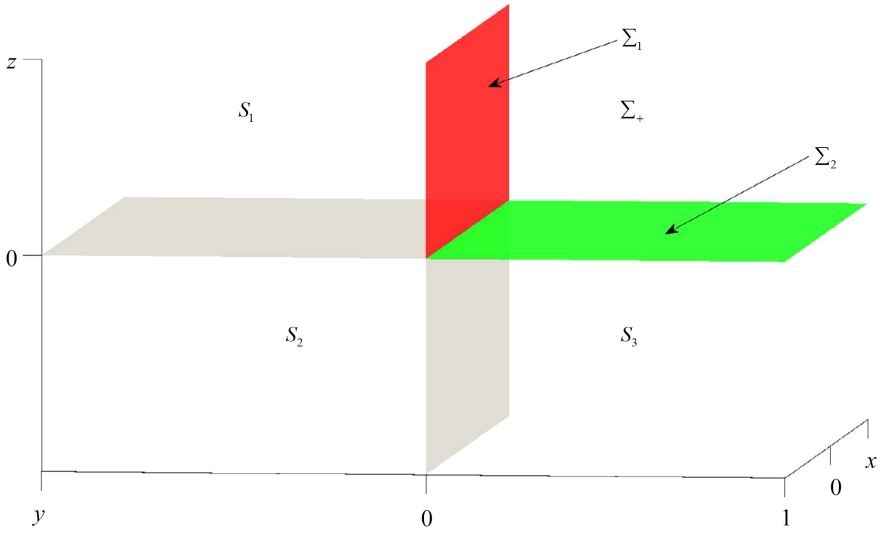

Figure 1. Graph of the switching manifold, $\Sigma_-=S_1\cup S_2\cup S_3$.

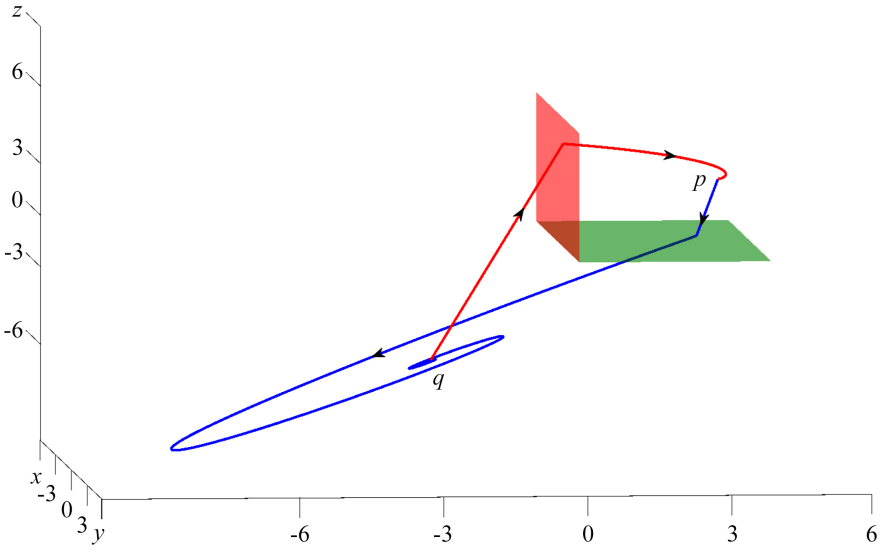

Figure 2. Graph of the heteroclinic cycle.

3)

$$\frac{\beta\sqrt{y_p^2+\delta_2^2}\,\mathrm{e}^{\alpha_1 t_0}}{\sqrt{\alpha_1^2+\beta_1^2}}<y_p,\ \frac{\beta\sqrt{\rho_1^2+\rho_2^2}\,\mathrm{e}^{\alpha t_1}}{\sqrt{\alpha_1^2+\beta_1^2}}<z_p,\ \frac{-\beta_2\sqrt{z_q^2+\sigma_1^2}\,\mathrm{e}^{\alpha_2 t_2}}{\sqrt{\alpha_2^2+\beta_2^2}}>z_q, \tag{15}$$

where

$$\begin{aligned} t_0&=\frac{1}{\beta_1}\left[\operatorname{arccot}\left(-\frac{\alpha_1}{\beta_1}\right)-\operatorname{arccot}\left(-\frac{\delta_2}{y_p}\right)+2\pi\right],\\ t_2&=\frac{1}{\beta_2}\left[\arctan\left(-\frac{\alpha_2}{\beta_2}\right)+\arcsin\left(\frac{z_q}{\sqrt{z_q^2+\sigma_1^2}}\right)+\pi\right], \end{aligned} \tag{16}$$

and if $\rho_1^2+\rho_2^2\neq 0$,

$$t_1=\begin{cases} \dfrac{1}{\beta_1}\left[\arctan\left(-\dfrac{\beta_1}{\alpha_1}\right)-\arcsin\left(\dfrac{\rho_1}{\sqrt{\rho_1^2+\rho_2^2}}\right)+\pi\right], & \rho_2\geq 0,\\ \dfrac{1}{\beta_1}\left[\arctan\left(-\dfrac{\beta_1}{\alpha_1}\right)-\arctan\left(\dfrac{\rho_1}{\rho_2}\right)\right], & \rho_2<0,\ \alpha_1\rho_1+\beta_1\rho_2\leq 0,\\ \dfrac{1}{\beta_1}\left[\arctan\left(-\dfrac{\beta_1}{\alpha_1}\right)-\arctan\left(\dfrac{\rho_1}{\rho_2}\right)+2\pi\right], & \rho_2<0,\ \alpha_1\rho_1+\beta_1\rho_2>0, \end{cases} \tag{17}$$

$$\delta_2=\zeta_{22}k_{10}-\zeta_{12}k_{20},\ \rho_1=\zeta_{13}k_{10}+\zeta_{23}k_{20}, \tag{18}$$

$$\rho_2=\zeta_{23}k_{10}-\zeta_{13}k_{20},\ \sigma_1=\xi_{23}l_{10}-\xi_{13}l_{20}. \tag{19}$$

Theorem 2. If system (1) satisfies the conditions of Theorem 1 and the eigenvalues of the matrices $\boldsymbol{A},\boldsymbol{B}$ satisfy

$$\lambda_1\lambda_2-\alpha_1\alpha_2>0,$$

then system (1) has infinite numbers of chaotic invariant sets.

4. The Proof of Theorem 1

If system (1) has a heteroclinic cycle connecting equilibrium points $\boldsymbol{q}$ and $\boldsymbol{p}$ that cross Σ transversely at two points, then one point is $\boldsymbol{p}_{11}=\boldsymbol{q}-\dfrac{y_p}{\xi_{32}}\xi_3$ and the other one is $\boldsymbol{p}_{02}=\boldsymbol{p}-\dfrac{z_p}{\zeta_{33}}\zeta_3$.

Consider the definition of heteroclinic cycles, system (1) has a heteroclinic cycle connecting $\boldsymbol{q}$ and $\boldsymbol{p}$ which crosses Σ_1 transversally at $\boldsymbol{p}_{11}$ and crosses Σ_2 transversally $\boldsymbol{p}_{02}$ if and only if the following conditions hold:

1) The positive orbit of $\boldsymbol{p}_{11}$ satisfies $\left\{\varphi_1(t,\boldsymbol{p}_{11})\,|\,t>0\right\}\subset\Sigma_+$.

2) The negative orbit of $\boldsymbol{p}_{11}$ satisfies $\left\{\varphi_2(t,\boldsymbol{p}_{11})\,|\,t<0\right\}\subset\Sigma_-$.

3) The positive orbit of $\boldsymbol{p}_{02}$ satisfies $\left\{\varphi_2(t,\boldsymbol{p}_{02})\,|\,t>0\right\}\subset\Sigma_-$.

4) The negative orbit of $\boldsymbol{p}_{02}$ satisfies $\left\{\varphi_2(t,\boldsymbol{p}_{02})\,|\,t<0\right\}\subset\Sigma_+$.

5) Transversal condition:

$$\begin{pmatrix}0 & 1 & 0\end{pmatrix}\left(\boldsymbol{A}\boldsymbol{p}_{11}+\boldsymbol{a}\right)\begin{pmatrix}0 & 1 & 0\end{pmatrix}\left(\boldsymbol{B}\boldsymbol{p}_{11}+\boldsymbol{b}\right)=0,$$

$$(0 \quad 0 \quad 1)(\boldsymbol{A}\boldsymbol{p}_{02}+\boldsymbol{a})(0 \quad 0 \quad 1)(\boldsymbol{B}\boldsymbol{p}_{02}+\boldsymbol{b})>0.$$

Since $\boldsymbol{p}_{02}\in W^u(\boldsymbol{p})$ and $\boldsymbol{p}_{11}\in W^u(\boldsymbol{q})$, then the negative orbit of $\boldsymbol{p}_{02}$ is a straight line connecting $\boldsymbol{p}_{02}$ and $\boldsymbol{p}$, the negative orbit of $\boldsymbol{p}_{11}$ is a straight line connecting $\boldsymbol{p}_{11}$ and $\boldsymbol{q}$. Hence,

$$\{\varphi_1(t,\boldsymbol{p}_{02})\,|\,t<0\}\subset\Sigma_+,\ \{\varphi_2(t,\boldsymbol{p}_{11})\,|\,t<0\}\subset\Sigma_-.$$

We will prove that the positive orbit of $\boldsymbol{p}_{11}$ satisfies $\{\varphi_1(t,\boldsymbol{p}_{11})\,|\,t>0\}\subset\Sigma_+$ which is equivalent to

$$(0\,1\,0)\varphi_1(t,\boldsymbol{p}_{11})>0,(0\,0\,1)\varphi_1(t,\boldsymbol{p}_{11})>0. \tag{20}$$

If $\rho_1^2+\rho_2^2=0$, then we have $(0\,0\,1)\varphi_1(t,\boldsymbol{p}_{11})=z_p>0$. And if $\rho_1^2+\rho_2^2\neq 0$, the inequalities in (20) are equivalent to

$$F_1(t)=\mathrm{e}^{\alpha_1 t}\sqrt{y_p^2+\delta_2^2}\sin(\theta_1+\beta_1 t)>-y_p,\ t>0, \tag{21}$$

and

$$F_2(t)=\mathrm{e}^{\alpha_1 t}\sqrt{\rho_1^2+\rho_2^2}\sin(\theta_2+\beta_1 t)>-z_p,\ t>0, \tag{22}$$

where

$$\sin\theta_1=\frac{-y_p}{\sqrt{y_p^2+\delta_2^2}}<0,\ \cos\theta_1=\frac{\delta_2}{\sqrt{y_p^2+\delta_2^2}}, \tag{23}$$

$$\sin\theta_2=\frac{\rho_1}{\sqrt{\rho_1^2+\rho_2^2}},\ \cos\theta_2=\frac{\rho_2}{\sqrt{\rho_1^2+\rho_2^2}}, \tag{24}$$

$$\delta_2=\zeta_{22}k_{10}-\zeta_{12}k_{20},\ \rho_1=\zeta_{13}k_{10}+\zeta_{23}k_{20},\ \rho_2=\zeta_{23}k_{10}-\zeta_{13}k_{20}. \tag{25}$$

Consider the expressions of $F_1(t)$ and $F_2(t)$, notice that $\alpha_1<0$, $\beta_1>0$, so the functions $F_1(t)$, $F_2(t)$ are the periodic oscillation attenuation functions and $F_1(t)$, $F_2(t)\to 0$ as $t\to+\infty$. To prove (21) and (22), we only need to consider the first local minimal points of the corresponding functions $F_1(t)$ and $F_2(t)$ in $\left[0,\frac{2\pi}{\beta_1}\right]$.

From (21)-(22), we have

$$F_1'(t)=\mathrm{e}^{\alpha_1 t}\sqrt{y_p^2+\delta_2^2}\left[\alpha\sin(\theta_1+\beta_1 t)+\beta\cos(\theta_1+\beta_1 t)\right] \tag{26}$$

$$F_1''(t)=\mathrm{e}^{\alpha_1 t}\sqrt{y_p^2+\delta_2^2}\left[(\alpha_1^2-\beta_1^2)\sin(\theta_1+\beta_1 t)+2\alpha_1\beta_1\cos(\theta_1+\beta_1 t)\right] \tag{27}$$

$$F_2'(t)=\mathrm{e}^{\alpha_1 t}\sqrt{\rho_1^2+\rho_2^2}\left[\alpha_1\sin(\theta_2+\beta_1 t)+\beta_1\cos(\theta_2+\beta_1 t)\right], \tag{28}$$

$$F_2''(t)=\mathrm{e}^{\alpha_1 t}\sqrt{\rho_1^2+\rho_2^2}\left[(\alpha_1^2-\beta_1^2)\sin(\theta_2+\beta_1 t)+2\alpha_1\beta_1\cos(\theta_2+\beta_1 t)\right], \tag{29}$$

$$F_1'(0)=-\alpha_1 y_p+\beta_1\delta_2,\ F_2'(0)=\alpha_1\rho_1+\beta_1\rho_2. \tag{30}$$

In the sequel, we will prove that $(0\,1\,0)\varphi_1(t,\boldsymbol{p}_{11})>0$ holds if and only if the second inequalities in (14) and the first inequality in (15) hold.

From (26), the local minimal points satisfy

$$F_1'(t)=0 \Leftrightarrow \cot(\theta_1+\beta_1 t)=-\frac{\alpha_1}{\beta_1}. \tag{31}$$

If t_0 satisfies Equation (31), then it satisfies

$$\sin(\theta_1+\beta_1 t_0)=\frac{-\beta_1}{\sqrt{\alpha_1^2+\beta_1^2}}<0,\ \cos(\theta_1+\beta_1 t_0)=\frac{\alpha_1}{\sqrt{\alpha_1^2+\beta_1^2}}<0, \tag{32}$$

or

$$\sin(\theta_1+\beta_1 t_0)=\frac{\beta_1}{\sqrt{\alpha_1^2+\beta_1^2}}>0,\ \cos(\theta_1+\beta_1 t_0)=\frac{-\alpha_1}{\sqrt{\alpha_1^2+\beta_1^2}}>0. \tag{33}$$

We can verify that and

$$F_1''(t_0)=-\mathrm{e}^{\alpha_1 t_0}\sqrt{y_p^2+\delta_2^2}\,\beta_1\left(\alpha_1^2+\beta_1^2\right)<0,$$

for t_0 satisfying Equation (33), so the t_0 satisfying Equation (33) is not local minimal points. And

$$F_1''(t_0)=\mathrm{e}^{\alpha_1 t_0}\sqrt{y_p^2+\delta_2^2}\,\beta_1\left(\alpha^2+\beta_1^2\right)>0,$$

for t_0 satisfying Equation (32), so $F_1(t)$ has the unique local minimal value in $\left[0,\frac{2\pi}{\beta_1}\right]$ at t_0 in (32) with

$$F_1(t_0)=\frac{-\beta_1\sqrt{y_p^2+\delta_2^2}\,\mathrm{e}^{\alpha_1 t_0}}{\sqrt{\alpha_1^2+\beta_1^2}}. \tag{34}$$

In addition, from Equations (32) and (23), we have

$$\beta_1 t_0+\theta_1=\operatorname{arccot}\left(-\frac{\alpha_1}{\beta_1}\right)+2k\pi+\pi,\ k\in Z,\ \theta_1=\pi+\operatorname{arccot}\left(-\frac{\delta_2}{y_p}\right),$$

then

$$\beta_1 t_0=\operatorname{arccot}\left(-\frac{\alpha_1}{\beta_1}\right)+2k\pi-\operatorname{arccot}\left(-\frac{\delta_2}{y_p}\right),\ k\in Z.$$

Since $F_1(0)=-y_p$ we must have $F_1'(0)=-\alpha_1 y_p+\beta_1\delta_2\geq 0$ to ensure $F_1(t)>-y_p$ for $t>0$. Moreover, consider the transversal condition $\begin{pmatrix}0 & 1 & 0\end{pmatrix}(\boldsymbol{A}\boldsymbol{p}_{11}+\boldsymbol{a})=-\alpha_1 y_p+\beta_1\delta_2\neq 0$, then we have $F_1'(0)=-\alpha_1 y_p+\beta_1\delta_2>0$. Thus

$$-\frac{\alpha_1}{\beta_1}>-\frac{\delta_2}{y_p}>0,$$

and we obtain that

$$\frac{\pi}{2}>\operatorname{arccot}\left(-\frac{\delta_2}{y_p}\right)>\operatorname{arccot}\left(-\frac{\alpha_1}{\beta_1}\right)>0.$$

Recall that $t_0\in\left(0,\frac{2\pi}{\beta_1}\right)$, we have

$$t_0 = \frac{1}{\beta_1}\left[\operatorname{arccot}\left(-\frac{\alpha_1}{\beta_1}\right) - \operatorname{arccot}\left(-\frac{\delta_2}{y_p}\right) + 2\pi\right].$$

Therefore, $(0\,1\,0)\varphi_1(t, \boldsymbol{p}_{11}) > 0$ holds for $t > 0$ if and only if the second inequality in (14) and the first inequality in (15) hold.

Next, we will prove that $(0\,0\,1)\varphi_1(t, \boldsymbol{p}_{11}) > 0$ holds $t > 0$ if and only if the third inequality in (14) and the second inequality in (15) hold. Consider the the first local minimal point t_1 of the function $F_2(t)$ in $\left[0, \frac{2\pi}{\beta_1}\right]$.

$$F_2'(t) = 0 \Leftrightarrow \tan(\theta_2 + \beta_1 t) = -\frac{\beta_1}{\alpha_1}. \tag{35}$$

Similar to the discussions of $F_1(t)$, the local minimal point t_1 of $F_2(t)$ in $\left[0, \frac{2\pi}{\beta_1}\right]$ satisfies

$$\sin(\theta_2 + \beta_1 t_1) = \frac{-\beta_1}{\sqrt{\alpha_1^2 + \beta_1^2}} < 0, \cos(\theta_2 + \beta_1 t_1) = \frac{\alpha_1}{\sqrt{\alpha_1^2 + \beta_1^2}} < 0, \tag{36}$$

and

$$F_2(t_1) = \frac{-\beta_1\sqrt{\rho_1^2 + \rho_2^2}\,\mathrm{e}^{\alpha_1 t_1}}{\sqrt{\alpha_1^2 + \beta_1^2}}. \tag{37}$$

To have $F_2(t) > -z_p$ for $t > 0$, we must have $F_2(0) = \zeta_{13}k_{10} + \zeta_{23}k_{20} = \rho_1 \geq -z_p$, which is the third inequality in (15). If $F_2(0) = \rho_1 = -z_p < 0$ similar to the discussions of $F_1(t)$, we must have $F_2'(0) = \alpha_1\rho_1 + \beta_1\rho_2 \geq 0$.

From Equation (36), we have

$$\beta_1 t_1 + \theta_2 = \arctan\left(-\frac{\beta_1}{\alpha_1}\right) + 2k\pi + \pi, \text{ with } k \in Z.$$

Consider formula (24), we have

$$\theta_2 = \arcsin\left(\frac{\rho_1}{\sqrt{\rho_1^2 + \rho_2^2}}\right),$$

for $\rho_2 \geq 0$, and

$$\theta_2 = \pi + \arctan\left(\frac{\rho_1}{\rho_2}\right),$$

for $\rho_2 < 0$. Then the local minimum point t_1 satisfies

$$\beta_1 t_1 = \arctan\left(-\frac{\beta_1}{\alpha_1}\right) + 2k\pi + \pi - \arcsin\left(\frac{\rho_1}{\sqrt{\rho_1^2 + \rho_2^2}}\right), \ k \in Z,$$

for $\rho_2 \geq 0$, and

$$\beta_1 t_1 = \arctan\left(-\frac{\beta_1}{\alpha_1}\right) + 2k\pi - \arctan\left(\frac{\rho_1}{\rho_2}\right), \ k \in Z,$$

for $\rho_2 < 0$.

Since $t_1 \in \left[0, \frac{2\pi}{\beta_1}\right]$, we have

$$t_1 = \frac{1}{\beta_1}\left[\arctan\left(-\frac{\beta_1}{\alpha_1}\right) - \arcsin\left(\frac{\rho_1}{\sqrt{\rho_1^2+\rho_2^2}}\right) + \pi\right],$$

for $\rho_2 \geq 0$. If $\rho_2 < 0$ and $\alpha_1\rho_1 + \beta_1\rho_2 \leq 0$, then we have

$$\tan\theta_1 = \frac{\rho_1}{\rho_2} \leq -\frac{\beta_1}{\alpha_1}.$$

Thus, we obtain that

$$-\frac{\pi}{2} < \arctan\left(\frac{\rho_1}{\rho_2}\right) \leq \arctan\left(-\frac{\beta_1}{\alpha_1}\right) < \frac{\pi}{2},$$

and

$$t_1 = \frac{1}{\beta_1}\left[\arctan\left(-\frac{\beta_1}{\alpha_1}\right) - \arctan\left(\frac{\rho_1}{\rho_2}\right)\right].$$

If $\rho_2 < 0$ and $\alpha_1\rho_1 + \beta_1\rho_2 > 0$, then we have

$$\tan\theta_1 = \frac{\rho_1}{\rho_2} > -\frac{\beta_1}{\alpha_1}.$$

Thus, we obtain that

$$\frac{\pi}{2} > \arctan\left(\frac{\rho_1}{\rho_2}\right) > \arctan\left(-\frac{\beta_1}{\alpha_1}\right) > 0,$$

and

$$t_1 = \frac{1}{\beta_1}\left[\arctan\left(-\frac{\beta_1}{\alpha_1}\right) - \arctan\left(\frac{\rho_1}{\rho_2}\right) + 2\pi\right].$$

Therefore, $(0\,0\,1)\varphi_1(t, \boldsymbol{p}_{11}) > 0$ holds for $t > 0$ if and only if the third inequality in (14) and the second inequality in (15) hold. Of course, using the aforementioned method, we can obtain the conditions for $\{\varphi_2(t, \boldsymbol{p}_{02}) \mid t < 0\} \subset \Sigma_+$.

From conditions of theorem (1), we have

$$(0 \quad 0 \quad 1)(\boldsymbol{A}\boldsymbol{p}_{02} + \boldsymbol{a}) = -z_p\lambda_1 < 0,$$

$$(0 \quad 0 \quad 1)(\boldsymbol{B}\boldsymbol{p}_{02} + \boldsymbol{b}) = -\alpha_2 z_q + \beta_2\sigma_1 < 0,$$

$$(0 \quad 1 \quad 0)(\boldsymbol{A}\boldsymbol{p}_{11} + \boldsymbol{a}) = -y_p\alpha_1 + \beta_1\delta_2 > 0,$$

$$(0 \quad 1 \quad 0)(\boldsymbol{B}\boldsymbol{p}_{11} + \boldsymbol{b}) = -\lambda_3 y_q > 0.$$

In conclusion, conditions 1) - 5) hold if and only if conditions in Theorem 1 hold. The proof of Theorem 1 is completed.

5. The Proof of Theorem 2

In this section, we will prove Theorem 2 through a two-step process based on

the methodology presented in reference [15].

Construct the Poincaré Map

At first, if system (1) fulfills the conditions stated in Theorem 1, it possesses a heteroclinic cycle Γ which connects the fixed points $\boldsymbol{p}$ and $\boldsymbol{q}$. This heteroclinic cycle Γ transversely intersects Σ_1 at the points $\boldsymbol{p}_{11}$ and transversely intersects Σ_1 at the points $\boldsymbol{p}_{02}$, as depicted in **Figure 2**.

For a small real constant number $\gamma_0 > 0$, let $y_1, y_2, y_3, y_4 \in (0, \gamma_0)$, and $y_2 < y_1$, $y_4 < y_3$, and

$$\Pi_1 = \left\{ \boldsymbol{p} + \begin{pmatrix} \zeta_1 & \zeta_2 & \zeta_3 \end{pmatrix} \begin{pmatrix} 0 \\ y \\ z \end{pmatrix} \middle| \, y_2 \le y \le y_1, 0 < z < \gamma_1 \right\},$$

$$\Pi_2 = \left\{ \boldsymbol{q} + \begin{pmatrix} \zeta_1 & \zeta_2 & \zeta_3 \end{pmatrix} \begin{pmatrix} 0 \\ y \\ z \end{pmatrix} \middle| \, y_4 \le y \le y_3, 0 < z < \gamma_2 \right\},$$

$$\Pi_3 = \left\{ \boldsymbol{p} + \begin{pmatrix} \zeta_1 & \zeta_2 & \zeta_3 \end{pmatrix} \begin{pmatrix} x \\ y \\ \gamma_3 \end{pmatrix} \middle| \, |x| \le \varepsilon_1, |y| < \varepsilon_1 \right\},$$

$$\Pi_4 = \left\{ \boldsymbol{q} + \begin{pmatrix} \zeta_1 & \zeta_2 & \zeta_3 \end{pmatrix} \begin{pmatrix} 0 \\ y \\ \gamma_4 \end{pmatrix} \middle| \, |x| \le \varepsilon_2, |y| < \varepsilon_2 \right\},$$

where $\gamma_1 > 0 > \gamma_3$, $0 < \gamma_2 < \gamma_4$ and $\varepsilon_1, \varepsilon_2 > 0$, they are small enough such that $\Pi_1, \Pi_3 \subset \Sigma_+$, $\Pi_2, \Pi_4 \subset \Sigma_-$. According to the aforementioned definition of the Poincaré sections Π_i, the heteroclinic cycle Γ intersects each Π_i at a single point for $i = 1, 2, 3, 4$. Suppose

$$X_5 = \Pi_1 \cap \Gamma, \ X_6 = \Pi_2 \cap \Gamma, \tag{38}$$

$$X_7 = \Pi_3 \cap \Gamma, \ X_8 = \Pi_4 \cap \Gamma. \tag{39}$$

then there exist $t_1, t_2 < 0$, $t_3, t_4 > 0$, such that

$$\varphi_1(t_1, X_5) = \boldsymbol{p}_{11}, \ \varphi_1(t_3, X_7) = \boldsymbol{p}_{02}, \tag{40}$$

$$\varphi_2(t_2, X_6) = \boldsymbol{p}_{02}, \ \varphi_2(t_4, X_8) = \boldsymbol{p}_{11}. \tag{41}$$

To create the Poincaré map of the system (1), we first require the subsequent outcomes.

Let's consider the mapping P_1 from Π_1 to Π_3. For a point

$$X = \boldsymbol{p} + P\begin{pmatrix} 0 & y & z \end{pmatrix}^{\mathrm{T}} \in \Pi_1,$$

$P_1(X)$ is defined as the first intersection of the trajectory $\varphi_1(t, X)$ with Π_3. By (10), we get $P_1 : \Pi_1 \to \Pi_3$

$$\boldsymbol{p}+P\begin{pmatrix}0\\ y\\ z\end{pmatrix}\mapsto \boldsymbol{p}+P\begin{pmatrix}-y\left(\frac{\gamma_3}{z}\right)^{\frac{\alpha_1}{\lambda_1}}\sin\left(\frac{\beta_1}{\lambda_1}\ln\left(\frac{\gamma_3}{z}\right)\right)\\ y\left(\frac{\gamma_3}{z}\right)^{\frac{\alpha_1}{\lambda_1}}\cos\left(\frac{\beta_1}{\lambda_1}\ln\left(\frac{\gamma_3}{z}\right)\right)\\ \gamma_3\end{pmatrix}. \tag{42}$$

Denote as

$$S_k=\left\{\boldsymbol{p}+P\begin{pmatrix}0 & y & z\end{pmatrix}^{\mathrm{T}} \mid y_2\le y\le y_1,\ \gamma_1\mathrm{e}^{\frac{-2(k+1)\pi\lambda_1}{\beta_1}}\le z\le\gamma_1\mathrm{e}^{\frac{-2k\pi\lambda_1}{\beta_1}}\right\}, \tag{43}$$

then we have

$$\Pi_1=\bigcup_{k=0}^{\infty}S_k.$$

Denote the upper boundary of S_k as h^u, the lower boundary of S_k as h^d, the left boundary of S_k as v_l, and the right boundary of S_k as v_r.

$$h^u=\left\{\boldsymbol{p}+P\begin{pmatrix}0 & y & z\end{pmatrix}^{\mathrm{T}} \mid y_2\le y\le y_1,\ z=\gamma_1\mathrm{e}^{\frac{-2k\pi\lambda_1}{\beta_1}}\right\},$$

$$h^d=\left\{\boldsymbol{p}+P\begin{pmatrix}0 & y & z\end{pmatrix}^{\mathrm{T}} \mid y_2\le y\le y_1,\ z=\gamma_1\mathrm{e}^{\frac{-2(k+1)\pi\lambda_1}{\beta_1}}\right\},$$

$$v^l=\left\{\boldsymbol{p}+P\begin{pmatrix}0 & y & z\end{pmatrix}^{\mathrm{T}} \mid y=y_2,\ \gamma_1\mathrm{e}^{\frac{-2(k+1)\pi\lambda_1}{\beta_1}}\le z\le\gamma_1\mathrm{e}^{\frac{-2k\pi\lambda_1}{\beta_1}}\right\},$$

$$v^r=\left\{\boldsymbol{p}+P\begin{pmatrix}0 & y & z\end{pmatrix}^{\mathrm{T}} \mid y=y_1,\ \gamma_1\mathrm{e}^{\frac{-2(k+1)\pi\lambda_1}{\beta_1}}\le z\le\gamma_1\mathrm{e}^{\frac{-2k\pi\lambda_1}{\beta_1}}\right\}.$$

Under the coordinate system $\{\boldsymbol{p};\zeta_1,\zeta_2,\zeta_3\}$, utilizing polar coordinates for the x and y components on Π_3, the transformation of the four boundaries by the function P_1 can be described as follows:

$$P_1\left(h^u\right)=\left\{(r,\theta)\mid\theta=-\frac{\beta_1}{\lambda_1}\ln\left(\frac{\gamma_3}{\gamma_1}\right)+2k\pi,\ r\in\left(y_2\left(\frac{\gamma_3}{\gamma_1}\right)^{\frac{\alpha_1}{\lambda_1}}\mathrm{e}^{\frac{2k\pi\alpha_1}{\beta_1}},y_1\left(\frac{\gamma_3}{\gamma_1}\right)^{\frac{\alpha_1}{\lambda_1}}\mathrm{e}^{\frac{2k\pi\alpha_1}{\beta_1}}\right)\right\},$$

$$P_1\left(h^d\right)=\left\{(r,\theta)\mid\theta=-\frac{\beta_1}{\lambda_1}\ln\left(\frac{\gamma_3}{\gamma_1}\right)+2(k+1)\pi,\ r\in\left(y_2\left(\frac{\gamma_3}{\gamma_1}\right)^{\frac{\alpha_1}{\lambda_1}}\mathrm{e}^{\frac{2(k+1)\pi\alpha_1}{\beta_1}},y_1\left(\frac{\gamma_3}{\gamma_1}\right)^{\frac{\alpha_1}{\lambda_1}}\mathrm{e}^{\frac{2(k+1)\pi\alpha_1}{\beta_1}}\right)\right\},$$

$$P_1\left(v^l\right)=\left\{(r,\theta)\,|\,\theta\in\left(-\frac{\beta_1}{\lambda_1}\ln\left(\frac{\gamma_3}{\gamma_1}\right)+2k\pi,-\frac{\beta_1}{\lambda_1}\ln\left(\frac{\gamma_3}{\gamma_1}\right)+2(k+1)\pi\right),\right.$$
$$\left.r\in\left(y_2\left(\frac{\gamma_3}{\gamma_1}\right)^{\frac{\alpha_1}{\lambda_1}}\mathrm{e}^{\frac{2(k+1)\pi\alpha_1}{\beta_1}},y_2\left(\frac{\gamma_3}{\gamma_1}\right)^{\frac{\alpha_1}{\lambda_1}}\mathrm{e}^{\frac{2k\pi\alpha_1}{\beta_1}}\right)\right\},$$

$$P_1\left(v^r\right)=\left\{(r,\theta)\,|\,\theta\in\left(-\frac{\beta_1}{\lambda_1}\ln\left(\frac{\gamma_3}{\gamma_1}\right)+2k\pi,-\frac{\beta_1}{\lambda_1}\ln\left(\frac{\gamma_3}{\gamma_1}\right)+2(k+1)\pi\right),\right.$$
$$\left.r\in\left(y_1\left(\frac{\gamma_3}{\gamma_1}\right)^{\frac{\alpha_1}{\lambda_1}}\mathrm{e}^{\frac{2(k+1)\pi\alpha_1}{\beta_1}},y_1\left(\frac{\gamma_3}{\gamma_1}\right)^{\frac{\alpha_1}{\lambda_1}}\mathrm{e}^{\frac{2k\pi\alpha_1}{\beta_1}}\right)\right\}.$$

From the above results, we have $r_{\max}=y_1\left(\frac{\gamma_3}{\gamma_1}\right)^{\frac{\alpha_1}{\lambda_1}}\mathrm{e}^{\frac{2k\pi\alpha_1}{\beta_1}}\to 0$, as $k\to\infty$.

For sufficiently large values of k, we have $P_1(S_k)\subset\Pi_3$. Based on the above calculations, we can roughly draw the graph of $P_1(S_k)$ as **Figure 3**. Using the same approach used to define P_1, we define the mapping P_2 from Π_2 to Π_4:

$$\boldsymbol{q}+Q\begin{pmatrix}0\\y\\z\end{pmatrix}\mapsto\boldsymbol{q}+Q\begin{pmatrix}-y\left(\frac{\gamma_4}{z}\right)^{\frac{\alpha_2}{\lambda_2}}\sin\left(\frac{\beta_2}{\lambda_2}\ln\left(\frac{\gamma_4}{z}\right)\right)\\ y\left(\frac{\gamma_4}{z}\right)^{\frac{\alpha_2}{\lambda_2}}\cos\left(\frac{\beta_2}{\lambda_2}\ln\left(\frac{\gamma_4}{z}\right)\right)\\ \gamma_4\end{pmatrix}.\tag{44}$$

Denote as

$$\overline{S}_n=\left\{\boldsymbol{q}+Q\begin{pmatrix}0&y&z\end{pmatrix}^{\mathrm{T}}\,|\,y_4\le y\le y_3,\gamma_2\mathrm{e}^{\frac{-2(n+1)\pi\lambda_2}{\beta_2}}\le z\le\gamma_2\mathrm{e}^{\frac{-2n\pi\lambda_2}{\beta_2}}\right\},\tag{45}$$

then we have

$$\Pi_2=\bigcup_{n=0}^{\infty}\overline{S}_n.$$

Similar to the representation of $P_1(S_k)$, when n is sufficiently large, we can roughly draw the graph of $P_2\left(\overline{S}_n\right)$ as **Figure 4**. Now, we introduce the mapping P_3 from Π_3 to Σ_2. Note that the flight time of a point

$$X=\boldsymbol{q}+P\begin{pmatrix}x&y&\gamma_3\end{pmatrix}^{\mathrm{T}}\in\Pi_3,$$

to reach Σ_2 corresponds to the largest negative solution of the equation

$$F_1(t,x,y)=\begin{pmatrix}0&0&1\end{pmatrix}\left[\mathrm{e}^{At}\left(X-\boldsymbol{p}\right)+\boldsymbol{p}\right]=0.\tag{46}$$

By the first equality of (39), X_7 can be expressed as

$$X_7=p+P\begin{pmatrix}0&0&\gamma_3\end{pmatrix}^{\mathrm{T}}\in\Pi_3.$$

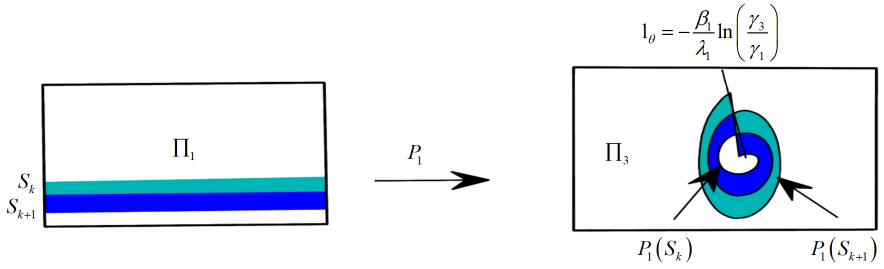

Figure 3. Geometric structure of P_1 and S_k.

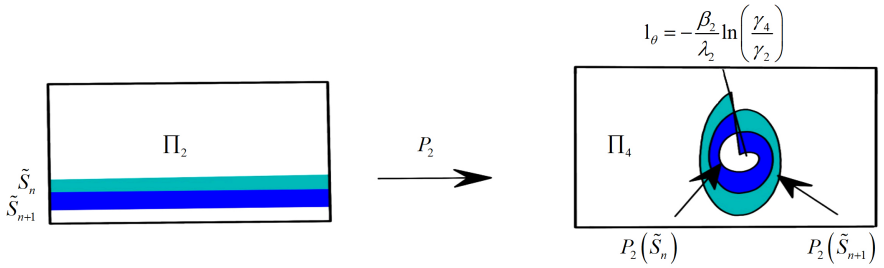

Figure 4. Geometric structure of P_2 and $\tilde{S}_n$.

Given the second equivalence in (40) $\boldsymbol{p}_{02} \in \Sigma_2$, we can conclude

$$F_1(t_3, 0, 0) = 0,$$

from (46), we have

$$t_3 = \frac{1}{\lambda_1}\ln\left(-\frac{z_p}{\zeta_{33}\gamma_3}\right),$$

$$F_1(t_3, 0, 0) = \lambda_1\zeta_{33}e^{\lambda_1 t_3} \neq 0.$$

Therefore, according to the implicit function theorem, there exists a neighborhood $\tilde{U}_1$ of X_7 such that

$$t(x, y) = t_3 + \tilde{k}_1 x + \tilde{k}_2 y + O(2),$$

where $\tilde{k}_1, \tilde{k}_2$ are constant real numbers.

Then, neglecting the $O(2)$ terms, the expression for P_3 is given by

$$\boldsymbol{p} + P\begin{pmatrix} x \\ y \\ \gamma_3 \end{pmatrix} \mapsto \boldsymbol{p}_{02} + PH_1\begin{pmatrix} x \\ y \\ 0 \end{pmatrix}, \tag{47}$$

where

$$H_1 = \begin{pmatrix} 1 & 0 & 0 \\ 0 & 1 & 0 \\ \frac{-\zeta_{13}}{\zeta_{33}} & \frac{-\zeta_{23}}{\zeta_{33}} & 0 \end{pmatrix}\begin{pmatrix} \mu_1 & -\nu_1 & 0 \\ \nu_1 & \mu_1 & 0 \\ 0 & 0 & 0 \end{pmatrix},$$

ν_1, μ_1 are constant real numbers.

Note that P_3 is an affine map. Using the same method to define P_3, we can also define the following map. The transformation P_4 from Π_4 to Σ_1. There

exists a neighborhood $\tilde{U}_2$ of X_8 such that the affine transformation P_4 is defined as

$$\boldsymbol{q}+Q\begin{pmatrix}x\\ y\\ \gamma_4\end{pmatrix}\mapsto \boldsymbol{p}_{11}+PH_2\begin{pmatrix}x\\ y\\ 0\end{pmatrix}, \tag{48}$$

where

$$H_2=\begin{pmatrix}1 & 0 & 0\\ \dfrac{-\zeta_{12}}{\zeta_{32}} & \dfrac{-\zeta_{22}}{\zeta_{32}} & 0\\ 0 & 1 & 0\end{pmatrix}\begin{pmatrix}\mu_2 & -\nu_2 & 0\\ \nu_2 & \mu_2 & 0\\ 0 & 0 & 0\end{pmatrix},$$

ν_2,μ_2 are constant real numbers.

The map P_5 from Π_2 to Σ_2. There exists a neighborhood $\tilde{U}_3$ of X_6 such that P_5:

$$\boldsymbol{q}+Q\begin{pmatrix}0\\ y\\ z\end{pmatrix}\mapsto \boldsymbol{p}_{02}+P\begin{pmatrix}0 & \tilde{a}_1 & \tilde{b}_1\\ 0 & \tilde{c}_1 & \tilde{d}_1\\ 0 & 0 & \tilde{e}_1\end{pmatrix}\begin{pmatrix}0\\ y\\ z\end{pmatrix}, \tag{49}$$

where $\tilde{a}_1,\tilde{b}_1,\tilde{c}_1,\tilde{d}_1,\tilde{e}_1$ are real constant numbers.

The map P_6 from Π_1 to Σ_1. There exists a neighborhood $\tilde{U}_4$ of X_5 such that P_6:

$$\boldsymbol{p}+P\begin{pmatrix}0\\ y\\ z\end{pmatrix}\mapsto \boldsymbol{p}_{11}+P\begin{pmatrix}0 & \tilde{a}_2 & \tilde{b}_2\\ 0 & \tilde{e}_2 & 0\\ 0 & \tilde{c}_2 & \tilde{d}_2\end{pmatrix}\begin{pmatrix}0\\ y\\ z\end{pmatrix}, \tag{50}$$

where $\tilde{a}_2,\tilde{b}_2,\tilde{c}_2,\tilde{d}_2,\tilde{e}_2$ are real constant numbers.

In the end, we construct the Poincaré map P as follows

$$P=P_6^{-1}\circ P_4\circ P_2\circ P_5^{-1}\circ P_3\circ P_1. \tag{51}$$

For convenience, let

$$M_1=P_5^{-1}\circ P_3\circ P_1:\Pi_1\to\Pi_2, \tag{52}$$

$$M_2=P_6^{-1}\circ P_4\circ P_2:\Pi_2\to\Pi_1, \tag{53}$$

then we have $P=M_2\circ M_1$.

Note that P_3,P_4,P_5, and P_6 are all affine mappings. Based on the diagrams of $P_1(S_k)$ and $P_2(\tilde{S}_n)$ shown in Figure 3 and Figure 4, we can select appropriate values of γ_1 and γ_2 such that $M_1(S_k)$ and $M_2(\tilde{S}_n)$ can be represented as shown in Figure 5 and Figure 6 for sufficiently large values of k and n.

Remark. Recalling Figure 3, under the mapping P_1, the right (resp. left) boundary of S_k is continuously mapped to the outer (resp. inner) boundary of an annulus-like object. Since the maps P_3 and P_5 are affine maps, the inner and outer boundaries of $P_1(S_k)$ correspond to the inner and outer boundaries of $M_1(S_k)$, respectively.

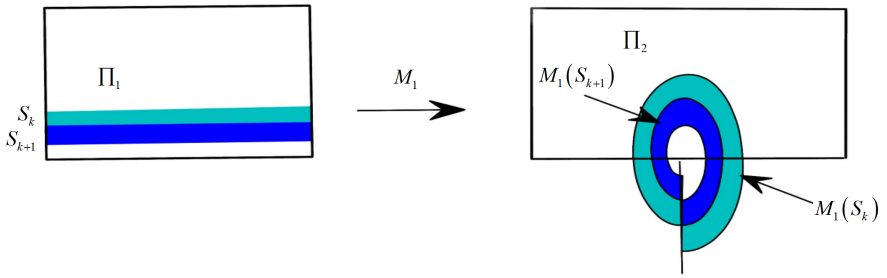

Figure 5. Geometric structure of M_1 and S_k.

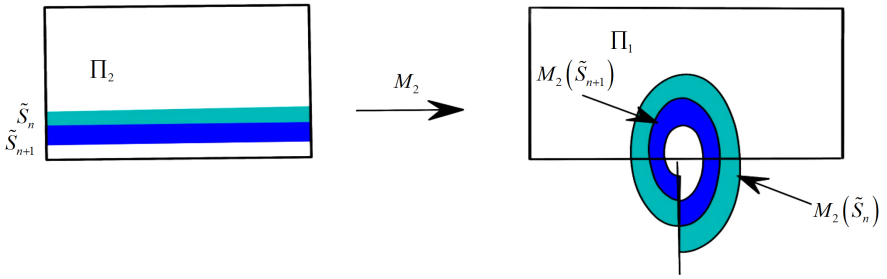

Figure 6. Geometric structure of M_2 and $\tilde{S}_k$.

Similarly, the inner and outer boundaries of $P_2(\tilde{S}_n)$ correspond to the respective inner and outer boundaries of $M_2(\tilde{S}_n)$.

Statement 1. Consider S_k for fixed k large enough, under the conditions of Theorem 2, there exists a positive integer n such that the inner boundary of $M_1(S_k)$ intersects the upper boundary of $\tilde{S}_n$ in two points, moreover, the inner boundary of $M_2(\tilde{S}_n)$ intersects the upper boundary of S_k in two points.

Proof: For fixed k large enough, any point in $M_1(S_k)$ can be expressed as

$$\boldsymbol{q} + Q(0 \quad \bar{y} \quad \bar{z})^{\mathrm{T}}. \tag{54}$$

For the points in $M_1(S_k)$ expressed above, there exists a constant T_1 such that the minimum value of $|\bar{z}|$ satisfies

$$\left|\bar{z}_{M_1}\right|_{\min} \geq T_1 \mathrm{e}^{\frac{2(k+1)\pi\alpha_1}{\beta_1}},$$

Let n be the integer part of the number

$$-\frac{\beta_2}{2\pi\lambda_2}\ln\left(\frac{T_1}{\gamma_2}\right) - \frac{\beta_2\alpha_1(k+1)}{\lambda_2\beta_1}.$$

According to the definition of $\tilde{S}_n$, the points in $\tilde{S}_n$ can be expressed using the same formula as (54). Therefore, the maximum value of $|\bar{z}|$ for points in $\tilde{S}_n$ can be determined

$$\left|\bar{z}_{\tilde{S}_n}\right|_{\max} = \gamma_2 \mathrm{e}^{\frac{-2n\pi\lambda_2}{\beta_2}} \leq \left|\bar{z}_{M_1}\right|_{\min}.$$

As a result, we can roughly draw in Figure 7 that the inner boundary of $M_1(S_k)$ intersects with the upper boundary of $\tilde{S}_n$ at two points.

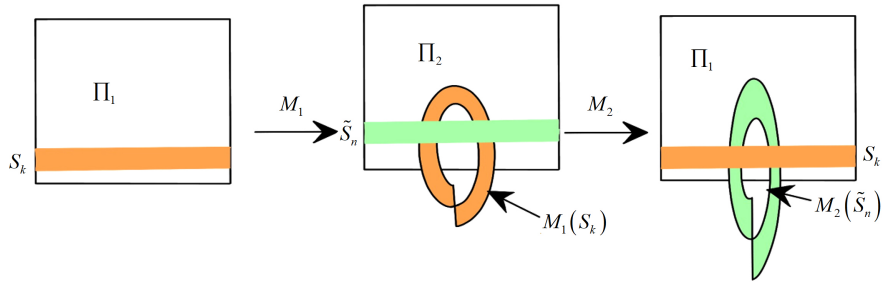

Figure 7. Geometric structure of S_k and $\tilde{S}_n$.

Consider points in $M_2(\tilde{S}_n)$, any point in $M_2(\tilde{S}_n)$ can be represented as follows

$$X = \boldsymbol{p} + P(0 \quad y \quad z)^{\mathrm{T}}, \tag{55}$$

for the smallest $|z|$, there exists a constant T_2,

$$|z_{M_2}|_{\min} \geq T_2 \mathrm{e}^{\frac{2(n+1)\pi\alpha_2}{\beta_2}},$$

On the other hand, the points S_k can be expressed in the same way as (55), and the largest absolute value of z S_k satisfies the following:

$$|z_{S_k}|_{\max} = \gamma_1 \mathrm{e}^{\frac{-2k\pi\lambda_1}{\beta_1}}.$$

Hence, if we can prove that

$$\frac{|z_{M_2}|_{\min}}{|z_{S_k}|_{\max}} > 1,$$

and we can roughly draw in **Figure 7** that the inner boundary of $M_2(\tilde{S}_n)$ intersects with the upper boundary of S_k at two points.

After performing straightforward calculations, we have

$$\frac{|z_{M_2}|_{\min}}{|z_{S_k}|_{\max}} = K\mathrm{e}^{\frac{2k\pi(\lambda_1\lambda_2-\alpha_1\alpha_2)}{\beta_1\lambda_2}}, \tag{56}$$

where

$$K = \frac{T_2}{\gamma_1}\left(\frac{\gamma_2}{T_2}\right)^{\frac{\alpha_2}{\lambda_2}} \mathrm{e}^{2\pi\left(\frac{\alpha_2}{\beta_2}-\frac{\alpha_1\alpha_2}{\beta_1\lambda_2}\right)}.$$

Consider the condition in Theorem 2: $\lambda_1\lambda_2 - \alpha_1\alpha_2 > 0$, then from (56), we get

$$\frac{|z_{M_2}|_{\min}}{|z_{S_k}|_{\max}} \to +\infty, \text{ as } k \to +\infty. \tag{57}$$

Consequently, for k large enough, $\frac{|z_{M_2}|_{\min}}{|z_{S_k}|_{\max}} > 1$.

Statement 2. For sufficiently large values of k, under the conditions of Corollary 2, S_k contains an invariant Cantor set on which the Poincaré map P is to-

pologically semiconjugate to a full shift on four symbols.

Proof: For sufficiently large values of k, according to Statement 1, there exists a positive integer n such that the intersection of $M_1(S_k)$ and $\tilde{S}_n$ consists of two small disjoint vertical strips in $\tilde{S}_n$, denoted as $\tilde{S}_{n1}$ and $\tilde{S}_{n1}$. In other words, we have

$$M_1(S_k) \cap \tilde{S}_n = \tilde{S}_{n1} \cup \tilde{S}_{n2},$$

and we can draw it as Figure 8. Based on Statement 1, we can conclude that the intersection of $M_2(\tilde{S}_n)$ and S_k consists of two small disjoint vertical strips in S_k, which are denoted by S_{ki1} and S_{ki2}. In other words:

$$M_2(\tilde{S}_{ni}) \cap S_k = S_{ki1} \cup S_{ki2}$$

for $i = 1, 2$.

According to Remark 6, the top and bottom edges of S_k represent the inner and outer edges of $M_1(S_k)$, respectively. Similarly, the top and bottom edges of $\tilde{S}_n$ represent the inner and outer edges of $M_2(\tilde{S}_n)$, respectively.

So, with respect to M_2, the primage of the left (resp, right) vertical boundary of S_{ki2} is included in the left (respectively, right) boundary of $\tilde{S}_{mi}$. Similarly, the primage of the left (respectively, right) vertical boundary of S_{ki1} is included in the right (respectively, left) boundary of $\tilde{S}_{ni}$, where $i = 1, 2$.

More importantly, in response to M_2, the primage of the two non-overlapping vertical strips S_{k22} and S_{k21} consists of two separate horizontal strips in $\tilde{S}_2$. Similarly, the primage of the two disjoint vertical strips S_{k11} and S_{k12} comprises two distinct horizontal strips in $\tilde{S}_{n1}$.

Let $\tilde{S}_{nij}$ represent the primage of S_{kij}, for $i, j = 1, 2$, as depicted in Figure 9.

Using a similar approach, we can conclude that the primage of the four horizontal strips associated with M_1 are four horizontal strips that are encompassed by S_k. Moreover, each horizontal strip intersects the upper and lower boundaries of S_{kij} at two distinct points, respectively, for $i, j = 1, 2$.

Denote by $\bar{S}_{kij}$ the primage of $\tilde{S}_{nij}$ corresponding to M_1, $i = 1, 2$, $j = 1, 2$, which is shown in Figure 9.

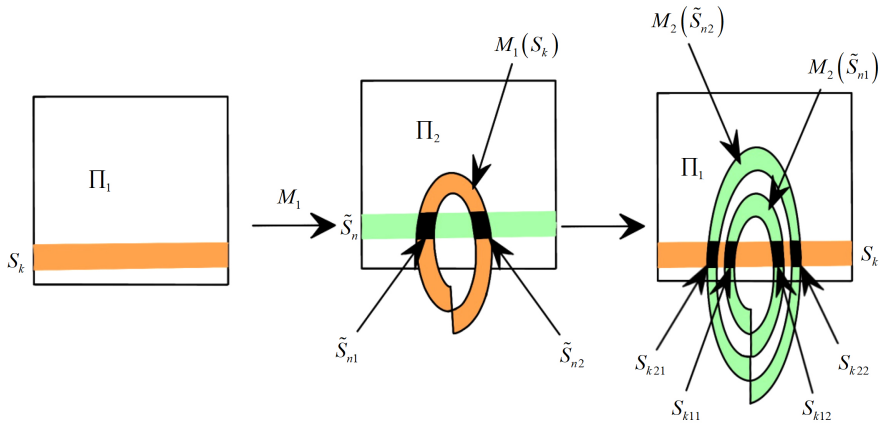

Figure 8. Geometric structure of S_{kij} and $\tilde{S}_{ni}$.

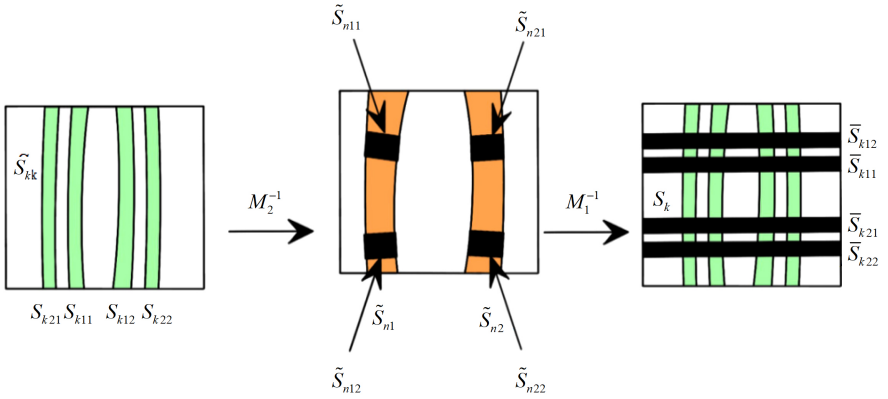

Figure 9. Geometric structure of $\bar{S}_{kij}$ and $\tilde{S}_n$.

Furthermore, it is evident that the left (resp, right) vertical edges of the primage $\bar{S}_{k22}$ and $\bar{S}_{k21}$ correspond to the left (resp, right) vertical edges of $\tilde{S}_{n22}$ and $\tilde{S}_{n21}$, respectively. Similarly, the left (resp, right) vertical edges of the primage $\bar{S}_{k12}$ and $\bar{S}_{k11}$ correspond to the right (resp, left) vertical edges of $\tilde{S}_{n12}$ and $\tilde{S}_{n12}$, respectively.

In summary, we can conclude that:

$$P\left(\bar{S}_{kij}\right) = S_{kij},$$

for $i = 1,2$, $j = 1,2$.

Additionally, it is clear that the left (resp, right, upper, lower) vertical boundaries of the primage $\bar{S}_{k22}$ and $\bar{S}_{k11}$ correspond to the left (respectively, right, upper, lower) vertical boundaries S_{k22} and S_{k11}, respectively. Similarly, the left (resp, right, upper, lower) vertical boundaries of the primage $\bar{S}_{k12}$ and $\bar{S}_{k21}$ correspond to the right (respectively, left, lower, upper) vertical boundaries S_{k12} and S_{k21}, respectively.

Then, by the Horse lemma, the proof is completed.

Remark. Based on the assertions made in Statements 1 and 2, the demonstration of Corollary 2 is finalized. In a manner akin to the Shil'nikov Theorems expounded in [12] [16] [17], it becomes apparent that system (1) possesses a minimum of an enumerable infinite number of chaotic invariant sets.

6. Conclusions

This paper proposes an analytical method on the existence of heteroclinic cycles in a class of 3-dimensional piecewise affine systems. Under the study of the corresponding chaotic dynamics, it provides a way to construct chaotic systems. Our method also can be applied to piecewise affine systems with more intricate switching planes, enabling the generation of multiple homoclinic or heteroclinic cycles. Additionally, it is feasible to produce multi-scroll chaotic attractors.

T his article conducts an analysis of the geometric structure of these systems, laying the groundwork for understanding how the types and positions of two equilibrium points, as well as changes in the geometric structure of invariant

manifolds, can affect the presence of singular cycles and chaos. The research presented in this article provides sufficient evidence to support the case where both equilibrium points are saddle-focus points and q is situated in the S_2 region. However, challenges still remain in studying other types of situations, necessitating further investigation by scientific researchers.

The existence of singular cycles and chaos in such systems can be influenced by various factors, including the types and positions of equilibrium points, as well as the geometric structure of invariant manifolds. To gain a comprehensive understanding and analysis of the behavior of these systems in more general scenarios, additional research is required.

Scientific researchers can continue to explore the dynamics of systems with different types of equilibrium points, investigating how changes in their positions can impact the presence of singular cycles and chaos. This may involve the development of novel mathematical techniques, conducting numerical simulations, or even experimental studies, depending on the specific characteristics of the system under investigation.

By addressing these unresolved challenges and conducting further research, scientists can deepen our comprehension of the dynamics exhibited by such systems, potentially uncovering new insights and phenomena. These advancements will contribute to the advancement of this field, fostering a more holistic understanding of complex dynamical behaviors.

Conflicts of Interest

The authors declare no conflicts of interest regarding the publication of this paper.

References

[1] Lorenz, E.N. (1963) Deterministic Nonperiodic Flow. *Journal of Atmospheric Sciences*, **20**, 130-141. https://doi.org/10.1175/1520-0469(1963)020<0130:DNF>2.0.CO;2

[2] Bernardo, M.D., Budd, C.J., Champneys, A.R. and Kowalczyk, P. (2008) Piecewise-Smooth Dynamical Systems: Theory and Applications. Springer Science and Business Media.

[3] Goebel, R., Sanfelice, R.G. and Teel, A.R. (2009) Hybrid Dynamical Systems. *IEEE Control Systems Magazine*, **29**, 28-93. https://doi.org/10.1109/MCS.2008.931718

[4] Huan, S.M., Li, Q.D. and Yang, X.-S. (2012) Chaos in Three-Dimensional Hybrid Systems and Design of Chaos Generators. *Nonlinear Dynamics*, **69**, 1915-1927. https://doi.org/10.1007/s11071-012-0396-0

[5] Alur, R., Courcoubetis, C., Halbwachs, N., Henzinger, T.A., Ho, P.H., Nicollin, X., Olivero, A., Sifakis, J. and Yovine, S. (1995) The Algorithmic Analysis of Hybrid Systems. *Theoretical Computer Science*, **138**, 3-34. https://doi.org/10.1016/0304-3975(94)00202-T

[6] Lin, H. and Antsaklis, P.J. (2014) Hybrid Dynamical Systems: An Introduction to Control and Verification. *Foundations and Trends in Systems and Control*, **1**, 1-172. https://doi.org/10.1561/2600000001

[7] Cao, Y., Chung, K. and Xu, J. (2011) A Novel Construction of Homoclinic and Heteroclinic Orbits in Nonlinear Oscillators by a Perturbation-Incremental Method. *Nonlinear Dynamics*, **64**, 221-236. https://doi.org/10.1007/s11071-011-9990-9

[8] Leonov, G.A. (2014) Fishing Principle for Homoclinic and Heteroclinic Trajectories. *Nonlinear Dynamics*, **78**, 2751-2758. https://doi.org/10.1007/s11071-014-1622-8

[9] Tigan, G. and Llibre, J. (2016) Heteroclinic, Homoclinic and Closed Orbits in the Chen System. *International Journal of Bifurcation and Chaos*, **26**, Article 1650072. https://doi.org/10.1142/S0218127416500723

[10] Tigan, G. and Turaev, D. (2011) Analytical Search for Homoclinic Bifurcations in the Shimizu-Morioka Model. *Physica D: Nonlinear Phenomena*, **240**, 895-989. https://doi.org/10.1016/j.physd.2011.02.013

[11] Lü, J.H. and Chen, G.R. (2006) Generating Multiscroll Chaotic Attractors: Theories, Methods and Applications. *International Journal of Bifurcation and Chaos*, **16**, 775-858. https://doi.org/10.1142/S0218127406015179

[12] Wang, F.R., Zhou, Z.C., Zhang, W. and Moroz, I. (2010) Coexistence of Three Heteroclinic Cycles and Chaos Analyses for a Class of 3d Piecewise Affine Systems. *Chaos: An Interdisciplinary Journal of Nonlinear Science*, **33**, Article 023108. https://doi.org/10.1063/5.0132018

[13] Carmona, V., Fernández-Sánchez, F., Garcia-Medina, E. and Teruel, A.E. (2010) Existence of Homoclinic Connections in Continuous Piecewise Linear Systems. *Chaos: An Interdisciplinary Journal of Nonlinear Science*, **20**, Article 013124. https://doi.org/10.1063/1.3339819

[14] Carmona, V., Fernández-Sánchez, F. and Garcia-Medina, E. (2017) Including Homoclinic Connections and T-Point Heteroclinic Cycles in the Same Global Problem for a Reversible Family of Piecewise Linear Systems. *Applied Mathematics and Computation*, **296**, 33-41. https://doi.org/10.1016/j.amc.2016.10.008

[15] Wu, T.T. and Yang, X.-S. (2016) Chaos Generator Design with Piecewise Affine Systems. *Nonlinear Dynamics*, **84**, 817-832. https://doi.org/10.1007/s11071-015-2529-8

[16] Kofman, E. (2004) Discrete Event Simulation of Hybrid Systems. *SIAM Journal on Scientific Computing*, **25**, 1771-1797. https://doi.org/10.1137/S1064827502418379

[17] Wu, T.T. and Yang, X.-S. (2016) A New Class of 3-Dimensional Piecewise Affine Systems with Homoclinic Orbits. *Discrete and Continuous Dynamical Systems*, **36**, 5119-5129. https://doi.org/10.3934/dcds.2016022

[18] Chen, Y.L., Wang, L. and Yang, X.-S. (2018) On the Existence of Heteroclinic Cycles in Some Class of 3-Dimensional Piecewise Affine Systems with Two Switching Planes. *Nonlinear Dynamics*, **91**, 67-79. https://doi.org/10.1007/s11071-017-3856-8

[19] Dong, H. and Zhang, T. (2021) External Bifurcations of Double Heterodimensional Cycles with One Orbit Flip. *Applied Mathematics*, **12**, 348-369. https://doi.org/10.4236/am.2021.124025

[20] Jin, Z. (2023) Crossing Limit Cycles of Planar Piecewise Hamiltonian Systems with Linear Centers Separated by Two Parallel Straight Lines. *Journal of Applied Mathematics and Physics*, **11**, 1429-1447. https://doi.org/10.4236/jamp.2023.115093

[21] Lu, K., Xu, W.J. and Yang, Q.G. (2020) Chaos Generated by a Class of 3d Three-Zone Piecewise Affine Systems with Coexisting Singular cycles. *International Journal of Bifurcation and Chaos*, **30**, Article 2050209.

https://doi.org/10.1142/S0218127420502090

[22] Lu, K. and Xu, W.J. (2022) Coexisting Singular Cycles in a Class of Three-Dimensional Three-Zone Piecewise Affine Systems. *Discrete and Continuous Dynamical Systems-Series B*, **27**, 7315-7349. https://doi.org/10.3934/dcdsb.2022045

[23] Lu, K., Xu, W.J., Yang, T. and Xiang, Q.M. (2022) Chaos Emerges from Coexisting Homoclinic Cycles for a Class of 3d Piecewise Systems. *Chaos*, *Solitons and Fractals*, **162**, Article 112470. https://doi.org/10.1016/j.chaos.2022.112470